

Cite this: *Energy Environ. Sci.*, 2011, **4**, 3494

www.rsc.org/ees

PAPER

The mechanism behind the beneficial effect of light soaking on injection efficiency and photocurrent in dye sensitized solar cells[†]

Andrea Listorti,^{*a} Charlotte Creager,^a Paul Sommeling,^b Jan Kroon,^b Emilio Palomares,^c Amparo Fornelli,^c Barry Breen,^d Piers R. F. Barnes,^a James R. Durrant,^a Chunhung Law^a and Brian O'Regan^{*a}

Received 9th April 2011, Accepted 2nd June 2011

DOI: 10.1039/c1ee01443a

Electrical and luminescence characterization was performed on 16 dye sensitized solar cells with different formulations, from different industrial and academic sources. Most of the cells were fabricated in pre-industrial pilot lines. The cells were put through a light soaking period up to 150 hours and then re-characterized. The results show the commonly observed increase in J_{sc} with light soaking is due to a decrease in the conduction band energy (with respect to the electrolyte) and an increase in the injection rate and efficiency. The strong correlation between the luminescence decay lifetime (<200 ps to 5 ns) and the photocurrent (7 to 13 mA cm⁻²) shows that the luminescence decay is a useful monitor of injection rates in these cells. The very slow injection shown by some cells implies substantial losses at the injection step. The data point to a need to understand and improve the TiO₂ processing and dyeing conditions in the industrial setting as well as the need to focus injection studies on the full range of dynamics present in the cells.

Introduction

Dye Sensitized Solar Cells (DSSC), a molecular approach to photovoltaic solar energy conversion, is one of the emerging solar technologies that offer the potential to reduce the cost of

photovoltaic electricity production. Over the last 20 years there has been extensive academic and, increasingly, commercial interest in this technology driven by the prospect of low start-up investment and low cost fabrication. Industrial prototyping is underway at a number of large and small entities; for example Corus (Tata) Steel in Europe and Sony in Asia. The latter has recently announced a mini-module with 8.4% energy efficiency. Over the last 20 years, there has been great progress in the materials components of such devices not only to enhance device efficiency, but also to improve stability and processability and to reduce production costs.^{1–5} In parallel with these materials advances, progress has been made in understanding the science of the processes underlying device performance.^{6–10} However the comprehension of such complex devices is still incomplete. There are complex interactions between the device components, in

^aDepartment of Chemistry, Imperial College London, London, SW7 2AZ, UK. E-mail: b.o'regan@imperial.ac.uk; a.listorti@imperial.ac.uk; Fax: +44 (0)207 594 5801; Tel: +44 (0)2075945031

^bEnergieonderzoek Centrum Nederland (ECN), Postbus 1, 1755 ZG Petten, The Netherlands

^cInstitut Català d'Investigació Química, (ICIQ), Avda. Països Catalans 16, Tarragona, Spain

^d3GSolar Ltd., 3 Hamarpe Street, AVX Building, Har Hozvim Industrial Park, Jerusalem, 97774, Israel

† Electronic supplementary information (ESI) available. See DOI: 10.1039/c1ee01443a

Broader context

DSSCs are “energy science” by virtue of their potential to be a commercial success. Yet the basic science underlying production and testing is underrepresented in the literature. Several standard procedures in the fabrication and testing of high efficiency DSSCs have effectively never been investigated. To cost effectively optimize production of DSSCs, as well as focus new research, one needs to understand the purpose of the steps which have been empirically added to the recipe. One such procedure is a few hours of exposure to light before measurement of the cell efficiency. Typically this “light soaking” causes an increase in the photocurrent. The procedure is common to most laboratories which make high efficiency cells, yet it is virtually never mentioned in the literature. For academia the procedure is not onerous, but in industry it presents a serious delay in quality control feedback. In this article, we examine the underlying mechanism of the light soaking effect. Doing so has conferred two benefits. First, the results are relevant to an ongoing debate on the kinetics of DSSCs. Second, the results may help point the way to cell fabrication procedures that avoid the need for the light soaking time, or methods of estimating the final efficiency without the time cost of light soaking.

particular at the oxide/dye/electrolyte interface, which control the kinetics of the forward and reverse reactions. As these kinetics in turn control the cell efficiency, a deeper understanding of the kinetics is of interest.

One of the intriguing observations made by several groups and industrial companies manufacturing DSSCs is a significant increase in the photocurrent during the first period of illumination. The phenomena have been observed in a wide range of cases, from small cells to large modules.^{11–20} The increase in photocurrent plateaus after a period of continuous illumination which can range from hours to days. This period of continuous illumination has been referred to as light soaking, and the increase is known as the “light soaking effect” (LSE). Light soaking has also been noted to cause a recovery of DSSC performance following a period of high temperature “accelerated aging”. Despite the importance of this effect, above all in manufacturing, there has been no systematic investigation of the cause.

In this paper we investigated the LSE on a number of cells from different research groups such as Energy Research Centre Netherlands (ECN), Institute of Chemical Research of Catalonia (ICIQ) and from an industrial company 3GSolar. With the exception of the ICIQ cells, the cells have been prepared using pilot scale production methods. Because of the requirements of speed and economy, the conditions of fabrication differ from those used to make record laboratory cells. We have measured the charge separation and charge collection kinetics on these cells before and after light soaking. From the results we propose that for these cells the increase in J_{sc} is due mainly to an increase in the electron injection rate from the excited dye to the TiO₂.

That this simple effect has not been noted before requires some explanation. We presume that the absence of studies of charge separation efficiency before and after light soaking stems from the perception that injection always occurs in the femtosecond time domain, and thus charge separation efficiency cannot be increased. This perception originates from early model system studies^{21–29} which indicated that electron injection from sensitizer dyes into metal oxides can occur on femtosecond timescales. Increasingly it has become apparent that photocurrent efficiencies lower than 100% can originate from slower electron injection rates.³⁰ In this paper we demonstrate the importance of the measuring injection rates in prototype devices aimed at large scale production.

Methods

1. Cell composition

We analysed 10 cells from ECN, with area 4 cm², employing two ruthenium based dyes: **Z907** and **C101**, and 3 different electrolytes: **EL1** (a.k.a. “maxell”; propionitrile with 0.6 M dimethylpropylimidazolium iodide, 0.5 M *N*-methylbenzimidazole, and 0.1 M iodine), **EL2** (a.k.a. Z946; 3-methoxypropionitrile (MPN) with 1.0 M dimethylimidazolium iodide (DMMI), 0.5 M *N*-butylbenzimidazole (NBB) 0.15 M iodine, and 0.1 M guanidinium thiocyanate), and **EL3** (a.k.a. Z646; identical to Z946 with propylmethylimidazolium iodide (PMMI) instead of DMMI). The TiO₂ layer thickness was 10 μm, with no scattering layer. A FTO:Pt counter electrode was used. We also analyzed

four cells from 3GSolar. These 2 cm² cells copy the composition and fabrication of the 3GSolar standard (250 cm²) cell. The TiO₂ film is 12 μm of DSL 18NR-T (Dyesol) with a 6 μm 3GSolar scattering. The 3GSolar cells employ **N719** as sensitizer. Two cells use SX AN50 (Solaronix) electrolyte and two have HSE electrolyte (Dyesol). And finally, two cells from ICIQ, 0.25 cm², employing **C101** dye with cheno as co-adsorbent, TiO₂ films of 9 μm DSL 18NR-T, **EL2** electrolyte, and a FTO/Pt cathode.

2. IV measurements and light soaking

The current–voltage characteristics of the cells were determined under illumination from a 150 W xenon lamp (Scientechnik model SS150Wsolar simulator), equipped with an IR filter (water filter) removing wavelengths >1000 nm and an AM 1.5 filter (Scientechnik). The intensity was adjusted using a calibrated silicon photodiode (model PBW21) to give an intensity approximately equivalent to that of a 100 mW cm^{−2} AM1.5G spectrum over the wavelength range of interest. The current and voltage were measured and controlled using a Keithley 2400 source meter. Light soaking was carried out under a 250 W fluorescent light source (Anko Solara) with an intensity that gave approximately the same photocurrent as the 1 sun simulator.

3. Charge density and luminescence lifetimes

We used the charge extraction technique to determine the concentration of electrons in the TiO₂ as a function of Fermi level position.^{31,32} Using our home designed TRACER (Transient and Charge Extraction) apparatus, the method is implemented as follows. The cell is placed at open circuit under a given white light intensity supplied using white LEDs. The V_{oc} in this case measures the Fermi level in the TiO₂ relative to the electrolyte potential. The latter is well buffered in our systems and is taken as constant. When the light is switched off and the cell is simultaneously short circuited the resulting discharge current of the TiO₂ chemical capacitance can be integrated to give a lower bound for the concentration of electrons in the TiO₂ prior to the switching. The LED lamps and cells can be switched in <1μs. By variation in the light intensity we vary the V_{oc} to build up the curve of electron density vs. Fermi level. We have verified that for standard DSSCs, charge extraction gives the same results as both the photoinduced absorption due to the electrons and the integration of the capacitance at V_{oc} from $V_{oc} = 0$ to V_{oc} at one sun. This capacitance can be determined via time resolved means such as impedance or transient photovoltages. We note the charge extraction experiment requires no assumptions or equivalent circuits and thus is more robust than the impedance methods. To determine changes in recombination and transport, photocurrent and photovoltage transients were also recorded using TRACER as described in previous works.^{33,34}

Luminescence lifetimes were used to estimate the electron injection efficiency of the excited dyes in each cell. The method is similar to that described in previous work.^{35–37} The luminescence lifetime was determined with a JobinYvon TBX Flurocube system with laser diode excitation at 467 nm, operating at 1 MHz and an average intensity of ~80 μW cm^{−2}. The instrument response function measured using the same experimental geometry was 200–250 ps full width half-maximum. The

photoluminescence decays were fit to a stretched exponential (eqn (1)) by convolution of the instrument response with the cell response. Residuals were in general evenly distributed. The average injection lifetime, τ_{obs} , was calculated for the stretched exponential using eqn (2). The average injection rate was taken as $1/\tau_{\text{obs}}$.

$$v = v_0 e^{-(t/\tau_{\text{ww}})^\beta} \quad (1)$$

$$\tau = \frac{\tau_{\text{ww}}}{\beta} \Gamma\left(\frac{1}{\beta}\right) \quad (2)$$

Luminescence lifetime in the absence of injection, τ_0 , was determined using control cells with the same dye and electrolyte but where the electron accepting TiO_2 has been replaced with ZrO_2 , considered to be a non-injecting substrate. The control cell luminescence decays were also fit to a stretched exponential giving an average lifetime τ_0 and rate, $1/\tau_0$, determined as above. We determined τ_0 for **C101** using control cells from ICIQ employing Z946 as electrolyte. For the **N719** cells from 3GSolar, exact control cells were not available and we have used τ_0 determined using ZrO_2 and an electrolyte consisting of acetonitrile/valeronitrile (85 : 15) with 0.6 M propylmethylimidazolium iodide (PMII), 0.04 M I_2 , 0.025 M LiI , 0.05 M guanidinium thiocyanate (GuSCN), 0.28 M 4-tertbutylpyridine (tBP)). For the τ_0 of **Z907** we used values from Koops and Durrant.³⁶ The slight differences between the working devices and the control cells may introduce some error which will be discussed below.

The quantum efficiency of electron injection, η_{inj} , *i.e.* the fraction of photons absorbed by the dye that are converted into electrons in the TiO_2 , can be written as:

$$\eta_{\text{inj}} = \frac{k_{\text{inj}}}{k_{\text{inj}} + k_0} \quad (3)$$

where k_{inj} represents the electron injection rate and k_0 represents the sum of all the alternative deactivation rates, such as radiative and non-radiative excited state deactivation. The injection quantum efficiency can be reformulated on the basis of our measured parameters as:

$$\eta_{\text{inj}} = \frac{1/\tau_{\text{obs}} - 1/\tau_0}{1/\tau_{\text{obs}}} \quad (4)$$

where $\tau_{\text{obs}} = 1/(k_{\text{inj}} + k_0)$ is the luminescence lifetime of the dye on the TiO_2 in the working cell and τ_0 is the lifetime in a control cell.^{35–37}

Results and discussion

Fig. 1 shows typical photocurrent *vs.* voltage (J - V) curves before and after light soaking. For all of the devices assembled at ECN and ICIQ we observed an increase in the photocurrent after light soaking treatment. The degree of increase was variable between cells, dependent on the electrolyte composition and employed dye. For example, the ECN devices employing **C101** show a larger increase than the ones employing **Z907**. In contrast, the four cells manufactured by 3GSolar, employing **N719**, showed no performance change, or change in the luminescence lifetime. Instead the four 3GSolar cells, with a combination of two different electrolytes and two different counter electrodes,

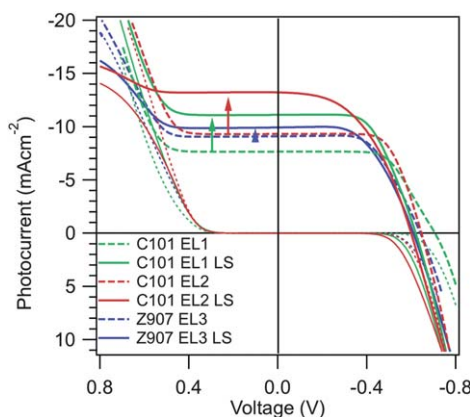


Fig. 1 Photocurrent–voltage curves of DSSCs employing the complex **C101** with electrolyte 1 (green), **C101** with electrolyte 2 (red) and **Z907** with electrolyte 3 (blue). The dashed lines are the photocurrent of the devices before the treatment and the solid lines are those of the devices after 150 hours of light soaking.

showed a clear trend in photocurrent with respect to cell composition (Fig. S1, ESI†). Unfortunately, the proprietary nature of the electrolyte used prevents us from speculating about the reasons for the lack of change with light soaking.

Fig. 2a shows the electron concentration (from the charge extraction measurements) plotted against V_{oc} , for 3 ECN devices before and after the light soaking treatment. The charge for these

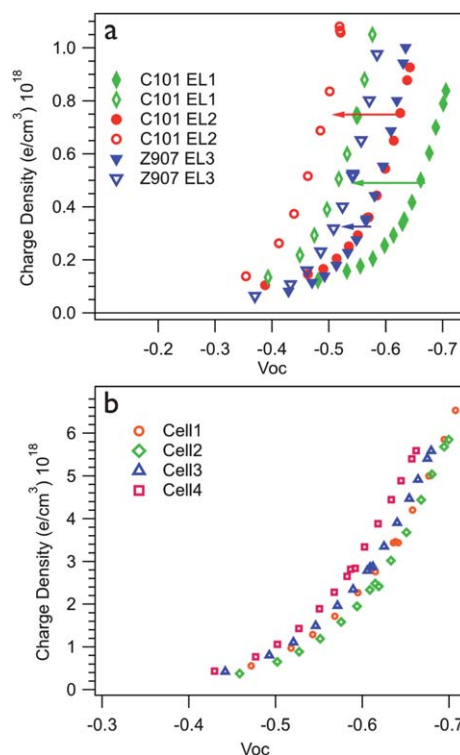


Fig. 2 (a) Charge density *vs.* V_{oc} for ECN DSSCs with the indicated dye and electrolyte. The full symbols represent the charge in the devices before the treatment and the empty ones are those of the devices after ~150 hours of light soaking. (b) Charge density *vs.* V_{oc} for the four 3GSolar DSSCs containing **N719** dye and two different electrolytes.

cells follows the typical exponential increase with voltage, $n = n_0 \exp(\gamma V_{oc})$ with $\gamma \sim 10$.

In the nanostructured TiO_2 films, the charge resides almost entirely in trap states in the band gap. In DSSCs with the standard electrolytes, such as the ones investigated here, the TiO_2 conduction band edge (CBE) is estimated to be about 1 Volt negative of the iodine/iodide redox potential. The iodine iodide redox potential is ~ 0.3 V positive of NHE thus the conduction band edge is ~ -0.7 V vs. NHE.

The CBE is thus well above the Fermi level at open circuit, which is ≤ 0.75 V for 1 sun illumination. The 0.25 V gap between the Fermi level and CBE results in minimal occupation of conduction band states. We assume for the following discussion that the trap states correspond to lattice defects and surface states that have a fixed energy with respect to the conduction band. We can interpret the changes in the electron density vs. V_{oc} curves in Fig. 2 as leftward shifts of the data (as shown by the arrows). This indicates a downward shift in the trap state energies towards the electrolyte redox potential with light soaking, and by extension a similar shift of the conduction band states and the CBE.

All cells which showed shifts in CBE with light soaking showed downshifts. Although this shift has been observed before,^{13,20,38} there is no convincing explanation offered as yet, nor do we attempt an explanation in this paper. Suffice it to note that the shift must be caused by a change in the surface dipole brought about by an increase in positive charge at the TiO_2 surface and/or a decrease in negative charge. We note that the CBE shift in many cells reverses with time in the dark, indicating it is not caused by permanent chemical breakdown of the electrolyte or dye. We also observe an increase in the recombination lifetime at V_{oc} ranging from 2 to 3 fold for **Z907**, and 3 to 6 fold for **C101**. The slowdown of recombination mitigates the loss of voltage associated with the decrease in the band edge (Fig. S2†).

In Fig. 2b the same charge concentration plot is reported for the four 3GSolar devices. There is a small downshift in the CBE along the series. Although there were no changes in the photocurrent with light soaking, the shift in the CBE between these cells correlates with the measured photocurrent, as discussed below.

Using the kind of data shown in Fig. 2, we can determine a set of relative CBEs for each group of cells with identical TiO_2 and fabrication procedure. For example, in Fig. 2 we can choose $6 \times 10^{18} \text{ cm}^{-3}$ as a reference electron concentration. Determining the voltage at which the charge density curve for each cell crosses $6 \times 10^{18} \text{ cm}^{-3}$ gives the relative conduction band edge for that cell. For the cells in Fig. 2a, this gives a range of 200 mV for the relative CBE, between 0.47 and 0.67 V. To convert this relative scale to an approximate absolute scale, we assume that the CBE of the average pre-light soaked cell lies at -1 V vs. the iodine/iodide potential in the electrolyte. This corresponds to 0.6 V on the relative scale above. Although -1 V vs. the electrolyte redox potential is a common estimate of the CBE, we keep the term approximate in using this scale due to the lack of certainty in this value.

Fig. 3 shows the short circuit current plotted against the approximate conduction band edge potential for the ECN and 3GSolar devices. The plot shows a linear increase in the photocurrent w/r to the CBE. For the ECN cells, the graph contains pairs of points, before and after light soaking. Some of these pairs are connected by arrows from the pre- to post-light soaking

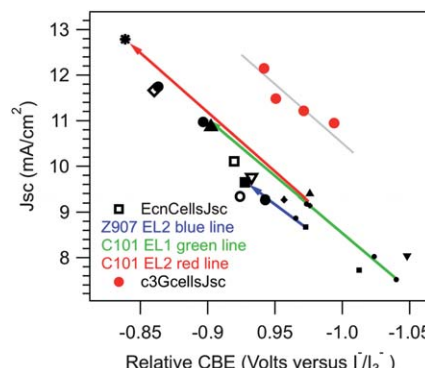


Fig. 3 Short circuit current *versus* approximate conduction band edge (CBE) potential (see text). Small filled symbols are pre-light soak values; large hollow symbols are post-light soaking for the same cell. Coloured arrows connect the pre- and post-light soaking points for 3 of the ECN cells.

points. The data in Fig. 3 include ECN cells with 2 different dyes and 3 different electrolytes. Although the dyes and electrolytes were not hugely different, it is still surprising that the CBE potential explains almost all the variation in the photocurrent shown by these cells.

The different TiO_2 preparation prevents direct comparison between the ECN and 3GSolar cells. However within the four 3GSolar cells there is a clear trend between the CBE potential and the photocurrent. One could even imagine that it had the same slope.

Fig. 4a shows typical luminescence decays of ECN DSSCs before and after the light soaking. The spread in decay times is already large before light soaking. The decay times clearly become shorter for the light soaked cells. Fig. 4b shows the luminescence decay of the four 3GSolar cells. The photocurrent is also given in the figure. The shorter decays are correlated with the higher photocurrents.

In the cells investigated for this report, we found a very wide distribution of τ_{obs} , ranging from a <200 ps to ~ 6 ns. Since τ_0 for the ruthenium dyes employed ranges from ~ 10 to ~ 30 nanoseconds, it is clear that the injection quantum efficiency will vary widely across the series. If these long luminescence decay times relate to the complete population of dye molecules, as opposed to some fraction of misplaced dyes, then the injection quantum efficiency should change in a reasonable way with respect to the changes in energy of the conduction band edge. Fig. 5 shows the relation of calculated η_{inj} (see Methods) with relative conduction band position for the ECN cells. The calculated efficiency increases with lower conduction band edge as expected. A lower conduction band edge, relative to I_3^-/I^- will also be a lower conduction band edge with respect to the energy of the excited dye. Because the density of states in TiO_2 increases with potential (be they trap or conduction band states), a lower CBE means a larger density of acceptor states in the TiO_2 iso-energetic with the dye excited state. This increases the rate at which the electron will be transferred to the TiO_2 .

In addition, the increase in efficiency plateaus at lower CBE as expected. Although the rate of electron injection can increase into the fs regime with lower conduction band energies, the efficiency increase cannot be accurately determined after the injection rate goes below $\sim 5\%$ of τ_0 . For the dyes used here-in,

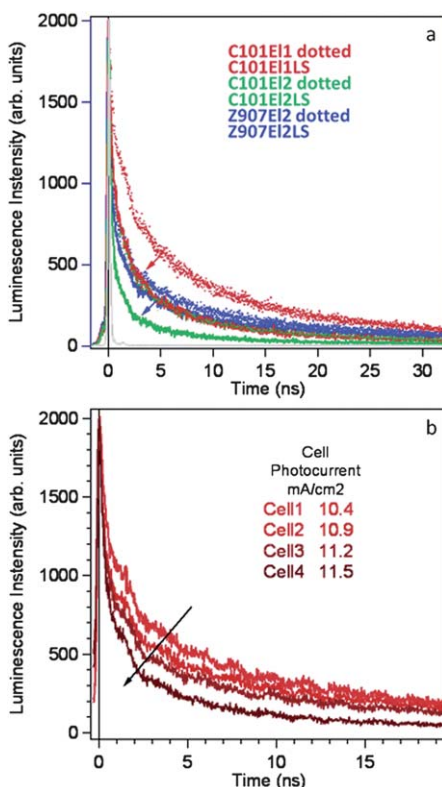


Fig. 4 (a) Transient emission decays of DSSCs employing the complex **C101** with electrolyte 1 (green), **C101** with electrolyte 2 (red) and **Z907** with electrolyte 2 (blue). The dotted lines are the emission decay of the devices before the treatment and the full lines are those of the devices after 150 hours of light soaking. (b) Transient emission decays and short circuit current values of 3GSolar devices, all of them employing **N719** ($\lambda_{\text{exc}} = 467 \text{ nm}$, $\lambda_{\text{det}} = 725 \text{ nm}$; IRF in light grey).

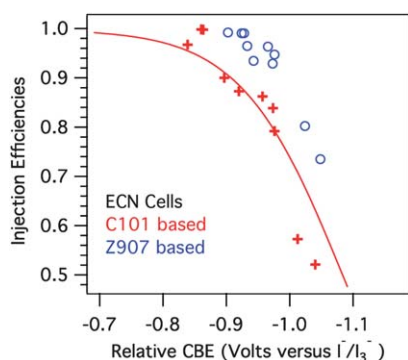


Fig. 5 Injection efficiencies versus relative conduction band edge (CBE) potentials (see text) for all the ECN devices.

that corresponds to an injection time $\leq 500 \text{ ps}$. The efficiency decrease as CBE increases follows a partial sigmoidal shape as expected. There is not enough data on the higher energy side to constrain a fit to theory. However, the data can be modelled by a Gaussian of dye energies injecting into an exponential density of trap states as reported in Koops *et al.*³⁵ This model is certainly not complete. For example, it does not recreate the observed stretched exponential. However it is also true that the data cannot be reproduced by a Gaussian distribution of dye energies

injecting into a parabolic CBE without an extremely small reorganization energy (width of the Gaussian $\leq 0.1 \text{ eV}$).

From the shift in the data in Fig. 5, it appears that cells made with the **Z907** dye can support a $\sim 60 \text{ mV}$ higher conduction band edge, relative to **C101** cells, before a significant decrease in injection efficiency occurs. This is partly due to the longer luminescence lifetime of **Z907** (20 ns) relative to **C101** (10 ns). In principle the increase in lifetime allows **Z907** to give $\sim 60 \text{ mV}$ higher V_{oc} when the CBE potential is fully optimized, assuming the recombination rate was similar for the two cells.

If the luminescence lifetime accurately reports on the injection rate constant for the majority of dyes, then the derived efficiency should correlate with the photocurrent, as long as collection efficiency is not also changing. The graphs in Fig. 6 show the correlation of the luminescence lifetime and the J_{sc} for each different set of cells. The correlation appears to be quite good. The line through the data is the predicted J_{sc} , calculated using eqn (5):

$$J_{\text{sc}} = J_{\max} \times \eta_{\text{inj}} \quad (5)$$

where J_{\max} is the J_{sc} that would occur in a cell with η_{inj} equal one. J_{\max} thus takes into account light absorption and current collection efficiency. In each panel the measured τ_0 (see above) is used so that J_{\max} is the only fit parameter. J_{\max} varies between panels due to different dyes and TiO_2 film thickness. With this one fit parameter we are able to explain most of the variation in the ECN cells. We note that in the ECN set there are three slightly different electrolytes which will give some variation in the real τ_0 . The fit is also remarkably good for the four 3GSolar cells. It is evident that changes in the injection rate account for $\sim 100\%$ of the difference between the 3GSolar cells even though they have two different electrolytes and different counter electrodes. In the ICIQ case there are only two cells, however the trend of

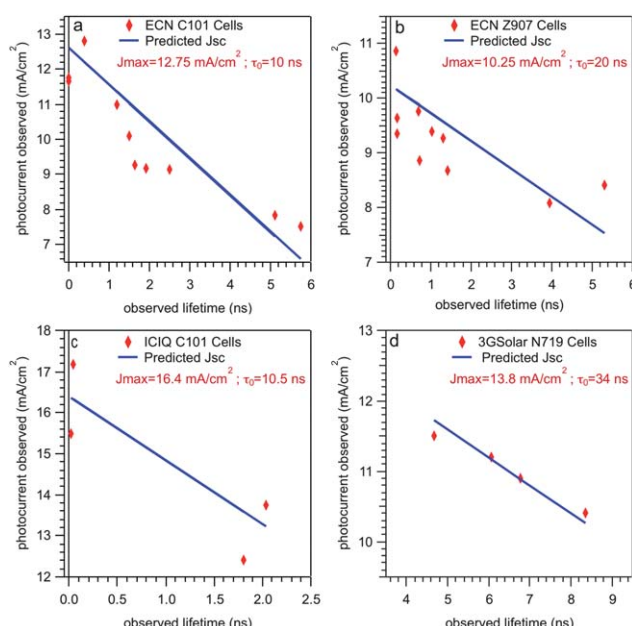


Fig. 6 Short circuit current versus observed luminescence lifetime. Lines through the data are one parameter fits using the J_{\max} and τ_0 given in the panel.

lifetime and J_{sc} are in general agreement. In several of the light soaked cells, the luminescence lifetime decreased to ≤ 100 ps, faster than the resolution of our TCSPC system. We note that the true rate for these points does not affect the correlations in Fig. 6 as the predicted photocurrent is effectively equal to J_{max} for any $\tau_{obs} \leq 200$ ps.

It might be argued that the TCSPC rate measures luminescence from some small fraction of the dyes, perhaps aggregates, which inject poorly, and therefore does not reflect the true injection rate of the majority of dyes. However, this argument cannot be made consistent with the trends in Fig. 6. Suppose, for example, 50% of the dyes are injecting in the femtosecond time range, giving a 100% efficiency for those dyes. Taking panel (a) these 50% of the dyes would give about 6.4 mA cm^{-2} both before and after light soaking. The injection efficiency of the other 50% of the dyes would have to change from 16 to 94% to accommodate the change in photocurrent across the plot. This would require a τ_0 for the aggregated dyes about 1/2 that measured on zirconia. We have measured the luminescence of the dye powder, the ultimate aggregate, and found it essentially the same as on zirconia. From this argument we feel that the TCSPC data in this paper measure the injection rate of the majority of dyes in these cells, leaving room for only a minority component in the femtosecond time scale.

One might still argue that the slow injection in these cells occurs because all the dyes are present as aggregates. However, it seems unlikely that all the aggregates would respond similarly to the decrease in band edge, unless all the aggregates were effectively identical. Moreover, if a dye aggregation does cause slow injection, it is presumably because of exciton migration from dyes not attached to TiO_2 to dyes which are attached. This energy diffusion process would not be very sensitive to the CBE potential, in contradiction to Fig. 5. It seems more reasonable to assume that in these cells, monomer dye layers are present and injecting slowly. This leaves open the question of why, in these cells, large amounts of light soaking are required to promote good injection, in comparison to others which function well with a more limited light soaking treatment.

This work may appear to be in contradiction to other work showing injection from excited dyes into TiO_2 occurs on the femtosecond timescale. On the other hand it is consistent with common knowledge that photocurrent is dependent on conduction band edge position.^{39–43} Fig. 7 shows an energy diagram that may shed some light on the discussion of slow and fast injection. In Fig. 7 we have drawn the conduction band edge CBE potential at the same level as the excited state of the N719 dye; both at -0.7 V vs. NHE . Although many articles show a $\sim 200 \text{ mV}$ driving force for injection in the same diagram, the available estimates of the two energy levels do not support this arrangement. In many articles, including most if not all articles about fast electron injection, the CBE edge position in “normal” cells is given as -0.5 V vs. NHE .^{7,10,40,44,45} The value is usually referenced to older DSSC references and is sometimes traceable back to DSSCs in water solution.^{26,46} If the CBE was in fact at -0.5 V vs. NHE , it would be at -0.8 V relative to the potential of the iodine/iodide couple in the organic electrolytes used. This seems unlikely, when the better DSSCs frequently have voltages of 0.77 V or more. This would place the Fermi level at the one sun V_{oc} less than 25 mV below the conduction band, resulting in

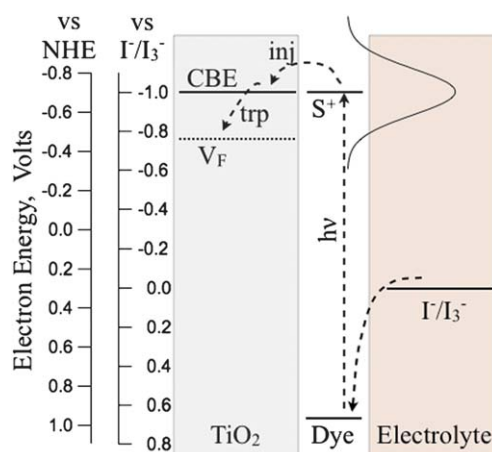


Fig. 7 Energy schematic of a typical high efficiency DSSC. The Z946 electrolyte is taken, where we measure the electrolyte redox potential to be $+0.30 \text{ V vs. NHE}$. The conduction band and dye energy levels are explained in the text. Electron injection (inj) is followed by trapping to the Fermi level (trp).

a very large electron density, as well as photovoltage saturation, neither of which is found in these cells.

However, in papers examining transport and recombination data from DSSCs the CBE potential is nearly always placed near -1 V vs. the electrolyte, or -0.7 V vs. NHE.^{34,47–51} The conduction band estimate in these papers is fixed by the need to model measured charge and transport data with reasonable values for the conduction band diffusion coefficient (D_o) and the effective density of states at the conduction band edge (N_c). The available values for D_o and N_c give CBE estimates -0.95 to -1.05 V in almost all publications. Because the measured redox potential of the electrolyte is $\sim 0.3 \text{ V}$ vs. NHE, the conduction band is thus at $\sim -0.7 \text{ V}$ vs. NHE. One commonly used estimate for the excited state potential of N719 is -0.65 to 0.7 V vs. NHE.⁷ This excited state value appears to derive from the oxidation potential of N3.⁵² There is some literature suggesting that the oxidation potential of N719 is less positive, however, with one exception,⁵³ these articles compare oxidation potentials measured in different labs and/or different periods. Ref. 53 attempted a direct comparison of N3 and N719 and found a more negative value for the latter. However, citing the complex and irreversible electrochemistry of N719, they were forced to use an *in situ* reduction of H^+ to H_2 to transiently de-protonate N3. More recent evidence indicates that, independent of the protonation state in the dye powder, the excited state potentials of N3 and N719 on the surface are identical.^{10,54,55}

Thus it appears that a reasonable estimate of the driving force for injection in optimized DSSCs could be zero, as depicted in Fig. 7. Of course, ΔG is not zero, because the argument above leaves out the larger density of states in the conduction band which adds an entropic contribution to ΔG . Electron trapping to the Fermi level adds another component to the complete injection process. Recalling that the potential for the excited state of the dye expresses the midpoint of the inhomogeneous broadening of this state, one can see that some of the dyes will be injecting “up hill” in the enthalpic sense, and thus the ns injection times measured here and elsewhere are consistent with what would be predicted. More broadly, it appears that the last 15 years of

optimization of both dyes (**N719** vs. **N3**) and electrolytes (optimization of base *vs.* lithium content) has been an effort to achieve exactly the situation depicted in Fig. 7. Given dyes which have long excited state lifetimes (*e.g.* 20 ns), optimization of the V_{oc} (by raising the conduction band) will terminate when the injection time reaches \sim 500 ps. We wish to note that neither our depiction in Fig. 7, nor those in other articles, should be taken very seriously. The energy levels of the dye are modulated by binding, and by its position inside the electrical double layer of the TiO_2 .⁵⁶ As the degree of modulation is not yet quantified, all figures like Fig. 7 are gross approximations.

We return to the apparent conflict of this work with the many studies showing a femtosecond (fs) rise in transient absorption in the range where the oxidized dye or the electron absorb. First, we note that the vast majority of fs studies are on films, not complete cells with base (*e.g.* TBP) in the electrolyte. However, some recent studies on films in base containing electrolytes do show a significant pico-second component that varies with electrolyte composition.^{57,58} Moreover, in ref. 57, there is good evidence of significant injection on the \geq 500 ps time scale. In this work, at 500 ps, the longest time measured, the transient absorbance spectrum indicates that at least 30% of the dyes are still in the excited state. This is evident because the relative absorption at 800 and 1200 nm at 500 ps is about 1 : 1,⁵⁷ whereas the ratio of dye cation (at 800 nm) to the electron (at 1200 nm) after complete injection is \sim 4 : 1.⁵⁹ The extra absorbance at 1200, identified as the remaining triplet states which have not yet injected, can be seen to be roughly 30% of the originally excited dyes.

The increase in injection rate with light soaking which we observe in this work also has implications for fs–ps transient absorption measurements. These measurements use intense, tightly focused, lasers leading to high incident powers. For example, in ref. 57 the pump laser intensity on the cell was equivalent to \sim 12 suns of white light, with additional light from the probe pulse.⁵⁷ Although DSSCs can operate at this intensity, this very high light soaking may accelerate some fraction of the injection into the fs–ps domain quite quickly. The measured rates would not correspond to the injection times under normal conditions.

This study is primarily about conditions present in pre-commercial cells. However, the results may also reflect the behaviour of “champion” cells. Recent reports on high efficiency ionic liquid based cells have also demonstrated a good correlation between ns luminescence lifetime and photocurrent.⁶⁰ The standard procedure for measuring champion cells also includes a period of light soaking in order to achieve maximum current. Assuming that these champion cells have the long diffusion lengths and high collection efficiencies normally claimed, the only way to realize an increase in current is by an increase in the injection rate. This implies that, before light soaking, some or all of the dyes in these champion cells have injection rates slow enough to create the observed loss. A lifetime longer than 2 ns is required to cause a 10% loss of injection for N719 and similar dyes. Clearly the photocurrent increase implies the average injection lifetime shortens into the ps range with light soaking, but there is no requirement that it reach fs to explain the photocurrent. If in fact a significant component of fs injection is found to be required in current champion cells, this identifies a problem rather than an advantage. The driving force required

to create a fs component of injection is a loss of energy to heat. If a fs component is required, presumably it is due to heterogeneity at the TiO_2 /dye interface resulting in a wide range of injection times. The conduction band position required to give efficient injection from the slower sites would then give fs injection from the faster sites. Thus the observation of fs injection should tell us we have not managed to control injection heterogeneity. A DSSC optimized with respect to electron injection would have a single injection lifetime, controlled by adjustment of the conduction band position to around 5% of the luminescence decay time (*e.g.* \sim 1 ns for N719). This would allow the maximum V_{oc} without significant loss of current. In sum, while studies of fs injection dynamics have high scientific appeal, by focussing only on the fs dynamics we may miss the opportunities for optimization that will come from understanding the full range of injection rates. On the other hand, if fs components are measured in high efficiency DSSCs, this gives hope for further increases in efficiency as they indicate the cells measured are still sub-optimum.

Conclusions

We find that the luminescence lifetime of dye sensitized solar cells from various sources, and before and after light soaking, correlates strongly with the photocurrent. Thus TCSPC can be used as a diagnostic tool for monitoring the quality of the TiO_2 surface and dye layer. We additionally find that the well known light soaking effect, whereby J_{sc} increases without large loss of voltage, is due to a decrease in the conduction band edge, an increase in the average injection rate, and a concomitant decrease in the recombination rate constant.

Acknowledgements

This work was supported by the European Union Robust DSC project (No. 212792).

Notes and references

- H. J. Snaith, A. J. Moule, C. Klein, K. Meerholz, R. H. Friend and M. Gratzel, *Nano Lett.*, 2007, **7**, 3372–3376.
- J. R. Durrant and M. Gratzel, in *Nanostructured and Photoelectrochemical Systems for Solar Photon Conversion*, ed. M. D. Archer and A. J. Nozik, Imperial College Press, London, 2008.
- A. Mishra, M. K. R. Fischer and P. Bauerle, *Angew. Chem., Int. Ed.*, 2009, **48**, 2474–2499.
- G. Boschloo and A. Hagfeldt, *Acc. Chem. Res.*, 2009, **42**, 1819–1826.
- S. Caramori, V. Cristina, R. Boaretto, R. Argazzi, C. A. Bignozzi and A. Di Carlo, *Int. J. Photoenergy*, 2010, 458614.
- J. N. Clifford, E. Martínez-Ferrero, A. Viterisi and E. Palomares, *Chem. Soc. Rev.*, 2011, **40**, 1635–1646.
- M. Gratzel, *Acc. Chem. Res.*, 2009, **42**, 1788–1798.
- B. C. O'Regan and J. R. Durrant, *Acc. Chem. Res.*, 2009, **42**, 1799–1808.
- S. Ardo and G. J. Meyer, *Chem. Soc. Rev.*, 2009, **38**, 115–164.
- A. Hagfeldt, G. Boschloo, L. C. Sun, L. Kloo and H. Pettersson, *Chem. Rev.*, 2010, **110**, 6595–6663.
- J. J. Kim, K. Lim, H. Choi, S. Fan, M. S. Kang, G. H. Gao, H. S. Kang and J. Ko, *Inorg. Chem.*, 2010, **49**, 8351–8357.
- B. O'Regan and D. T. Schwartz, *Chem. Mater.*, 1998, **10**, 1501–1509.
- S. Ferrere and B. A. Gregg, *J. Phys. Chem. B*, 2001, **105**, 7602–7605.
- B. A. Gregg, S. G. Chen and S. Ferrere, *J. Phys. Chem. B*, 2003, **107**, 3019–3029.
- A. Hinsch, J. M. Kroon, R. Kern, I. Uhlendorf, J. Holzbock, A. Meyer and J. Ferber, *Progr. Photovolt.: Res. Appl.*, 2001, **9**, 425–438.

- 16 D. B. Kuang, S. Ito, B. Wenger, C. Klein, J. E. Moser, R. Humphry-Baker, S. M. Zakeeruddin and M. Gratzel, *J. Am. Chem. Soc.*, 2006, **128**, 4146–4154.
- 17 K. M. Lee, S. J. Wu, C. Y. Chen, C. G. Wu, M. Ikegami, K. Miyoshi, T. Miyasaka and K. C. Ho, *J. Mater. Chem.*, 2009, **19**, 5009–5015.
- 18 H. Pettersson, T. Gruszecki, C. Schnetz, M. Streit, Y. H. Xu, L. C. Sun, M. Gorlov, L. Kloof, G. Boschloo, L. Haggman and A. Hagfeldt, *Progr. Photovolt.: Res. Appl.*, 2010, **18**, 340–345.
- 19 Q. Wang, Z. P. Zhang, S. M. Zakeeruddin and M. Gratzel, *J. Phys. Chem. C*, 2008, **112**, 10585.
- 20 Z. S. Wang, Y. Cui, Y. Dan-Oh, C. Kasada, A. Shinpo and K. Hara, *J. Phys. Chem. C*, 2008, **112**, 17011–17017.
- 21 J. B. Asbury, R. J. Ellingson, H. N. Ghosh, S. Ferrere, A. J. Nozik and T. Q. Lian, *J. Phys. Chem. B*, 1999, **103**, 3110–3119.
- 22 J. B. Asbury, E. Hao, Y. Q. Wang, H. N. Ghosh and T. Q. Lian, *J. Phys. Chem. B*, 2001, **105**, 4545–4557.
- 23 R. J. Ellingson, J. B. Asbury, S. Ferrere, H. N. Ghosh, J. R. Sprague, T. Q. Lian and A. J. Nozik, *J. Phys. Chem. B*, 1998, **102**, 6455–6458.
- 24 H. N. Ghosh, J. B. Asbury and T. Q. Lian, *J. Phys. Chem. B*, 1998, **102**, 6482–6486.
- 25 J. Kallioinen, G. Benko, V. Sundstrom, J. E. I. Korppi-Tommola and A. P. Yartsev, *J. Phys. Chem. B*, 2002, **106**, 4396–4404.
- 26 J. E. Moser and M. Gratzel, *Chem. Phys.*, 1993, **176**, 493–500.
- 27 J. E. Moser and M. Gratzel, *Chimia*, 1998, **52**, 160–162.
- 28 S. Pelet, M. Gratzel and J. E. Moser, *J. Phys. Chem. B*, 2003, **107**, 3215–3224.
- 29 Y. Tachibana, J. E. Moser, M. Gratzel, D. R. Klug and J. R. Durrant, *J. Phys. Chem.*, 1996, **100**, 20056–20062.
- 30 K. Hara, T. Sato, R. Katoh, A. Furube, Y. Ohga, A. Shinpo, S. Suga, K. Sayama, H. Sugihara and H. Arakawa, *J. Phys. Chem. B*, 2003, **107**, 597–606.
- 31 B. C. O'Regan, K. Bakker, J. Kroese, H. Smit, P. Sommeling and J. R. Durrant, *J. Phys. Chem. B*, 2006, **110**, 17155–17160.
- 32 P. R. F. Barnes, Y. A. Anderson, J. Mindaugas, L. Lingxuan, L. Xiaoe, E. Palomares, A. Fornelli and B. C. O'Regan, *Phys. Chem. Chem. Phys.*, 2011, **13**, 3547.
- 33 C. Law, S. C. Pathirana, X. Li, A. Y. Anderson, P. R. F. Barnes, A. Listorti, T. H. Ghaddar and B. C. O'Regan, *Adv. Mater.*, 2010, **22**, 4505–4509.
- 34 B. C. O'Regan, J. R. Durrant, P. M. Sommeling and N. J. Bakker, *J. Phys. Chem. C*, 2007, **111**, 14001–14010.
- 35 S. E. Koops, B. C. O'Regan, P. R. F. Barnes and J. R. Durrant, *J. Am. Chem. Soc.*, 2009, **131**, 4808–4818.
- 36 S. E. Koops and J. R. Durrant, *Inorg. Chim. Acta*, 2008, **361**, 663–670.
- 37 A. Listorti, I. Lopez-Duarte, M. V. Martinez-Diaz, T. Torres, T. Dos Santos, P. R. F. Barnes and J. R. Durrant, *Energy Environ. Sci.*, 2010, **3**, 1573–1579.
- 38 J. H. Yum, R. Humphry-Baker, S. M. Zakeeruddin, M. K. Nazeeruddin and M. Gratzel, *Nano Today*, 2010, **5**, 91–98.
- 39 C. A. Kelly, F. Farzad, D. W. Thompson, J. M. Stipkala and G. J. Meyer, *Langmuir*, 1999, **15**, 7047–7054.
- 40 J. B. Asbury, N. A. Anderson, E. C. Hao, X. Ai and T. Q. Lian, *J. Phys. Chem. B*, 2003, **107**, 7376–7386.
- 41 N. G. Park, S. H. Chang, J. van de Lagemaat, K. J. Kim and A. J. Frank, *Bull. Korean Chem. Soc.*, 2000, **21**, 985–988.
- 42 D. F. Watson and G. J. Meyer, *Coord. Chem. Rev.*, 2004, **248**, 1391–1406.
- 43 Y. Tachibana, S. A. Haque, I. P. Mercer, J. E. Moser, D. R. Klug and J. R. Durrant, *J. Phys. Chem. B*, 2001, **105**, 7424–7431.
- 44 K. Hara, Z. S. Wang, T. Sato, A. Furube, R. Katoh, H. Sugihara, Y. Dan-Oh, C. Kasada, A. Shinpo and S. Suga, *J. Phys. Chem. B*, 2005, **109**, 15476–15482.
- 45 R. Katoh, A. Furube, M. Murai, Y. Tamaki, K. Hara and M. Tachiya, *C. R. Chim.*, 2006, **9**, 639–644.
- 46 J. M. Rehm, G. L. McLendon, Y. Nagasawa, K. Yoshihara, J. Moser and M. Gratzel, *J. Phys. Chem.*, 1996, **100**, 9577–9578.
- 47 J. Villanueva, J. A. Anta, E. Guillen and G. Oskam, *J. Phys. Chem. C*, 2009, **113**, 19722–19731.
- 48 L. M. Peter, A. B. Walker, G. Boschloo and A. Hagfeldt, *J. Phys. Chem. B*, 2006, **110**, 13694–13699.
- 49 M. Quintana, T. Edvinsson, A. Hagfeldt and G. Boschloo, *J. Phys. Chem. C*, 2007, **111**, 1035–1041.
- 50 J. J. Lee, G. M. Coia and N. S. Lewis, *J. Phys. Chem. B*, 2004, **108**, 5282–5293.
- 51 M. Wang, P. Chen, R. Humphry-Baker, S. M. Zakeeruddin and M. Gratzel, *ChemPhysChem*, 2009, **10**, 290–299.
- 52 M. K. Nazeeruddin, A. Kay, I. Rodicio, R. Humphrybaker, E. Muller, P. Liska, N. Vlachopoulos and M. Gratzel, *J. Am. Chem. Soc.*, 1993, **115**, 6382–6390.
- 53 G. Wolfbauer, A. M. Bond, G. B. Deacon, D. R. MacFarlane and L. Spiccia, *J. Am. Chem. Soc.*, 2000, **122**, 130–142.
- 54 G. Boschloo and A. Hagfeldt, *Acc. Chem. Res.*, 2009, **42**, 1819–1826 (see page 1821).
- 55 F. De Angelis, S. Fantacci, E. Mosconi, M. K. Nazeeruddin and M. Gratzel, *J. Phys. Chem. C*, 2011, **115**, 8825–8831.
- 56 U. B. Cappel, S. M. Feldt, J. Schoneboom, A. Hagfeldt and G. Boschloo, *J. Am. Chem. Soc.*, 2010, **132**, 9096–9101.
- 57 A. Furube, Z. S. Wang, K. Sunahara, K. Hara, R. Katoh and M. Tachiya, *J. Am. Chem. Soc.*, 2010, **132**, 6614–6615.
- 58 J. J. H. Pijpers, R. Ulbricht, S. Derossi, J. N. H. Reek and M. Bonn, *J. Phys. Chem. C*, 2010, **115**, 2578–2584.
- 59 A. Y. Anderson, P. R. F. Barnes, J. R. Durrant and B. C. O'Regan, *J. Phys. Chem. C*, 2010, **114**, 1953–1958.
- 60 Y. Bai, J. Zhang, Y. H. Wang, M. Zhang and P. Wang, *Langmuir*, 2011, **27**, 4749–4755.